Cerebral Cortex March 2011;21:563-573
doi:10.1093/cercor/bhq123
Advance Access publication July 12, 2010

Response Dynamics and Tilt versus Translation Discrimination in Parietoinsular Vestibular Cortex

Sheng Liu, J. David Dickman and Dora E. Angelaki

Department of Neurobiology, Washington University School of Medicine, St Louis, MO 63110, USA

Address correspondence to Dr Dora Angelaki, Department of Anatomy and Neurobiology, Box 8108, Washington University School of Medicine, 660 South Euclid Avenue, St Louis MO 63110, USA. Email: angelaki@cabernet.wustl.edu.

The parietoinsular vestibular cortex (PIVC) is a large area in the lateral sulcus with neurons that respond to vestibular stimulation. Here we compare the properties of PIVC cells with those of neurons in brain stem, cerebellum, and thalamus. Most PIVC cells modulated during both translational and rotational head motion. Translation acceleration gains showed a modest decrease as stimulus frequency increased, with a steeper slope than that reported previously for thalamic and cerebellar nuclei neurons. Response dynamics during yaw rotation were similar to those reported for vestibular neurons in brain stem and thalamus: velocity gains were relatively flat through the mid-frequency range, increased at high frequencies, and decreased at low frequencies. Tilt dynamics were more variable: PIVC neurons responsive only to rotation had gains that decreased with increased frequency, whereas neurons responsive during both translation and rotation (convergent neurons) actually increased their modulation magnitude at high frequencies. Using combinations of translation and tilt, most PIVC neurons were better correlated with translational motion; only 14% were better correlated with net acceleration. Thus, although yaw rotation responses in PIVC appear little processed compared with other central vestibular neurons, translation and tilt responses suggest a further processing of linear acceleration signals in thalamocortical circuits.

Keywords: computation, cortex, lateral sulcus, PIVC, rotation, translation, vestibular

Introduction

How vestibular information is represented and processed in the cerebral cortex remains poorly understood, in contrast to other sensory systems. Early descriptions of vestibular cortical areas were based on evoked potentials following electrical stimulation of the vestibular nerve. For example, Fredrickson et al. (1966) described vestibular activation in the macaque area 2v, which is located at the lower tip of the intraparietal sulcus in the immediate vicinity of areas 5 and 7. Subsequent single-neuron recordings described vestibular modulation in this area, both in anesthetized (Fredrickson et al. 1966; Schwarz and Fredrickson 1971; Kornhuber 1972) and alert monkeys (Büttner and Buettner 1978). Around the same time, Odkvist et al. (1974) also described vestibular responses in a relatively restricted field of somatosensory area 3a in the squirrel monkey. More recently, neurons responsive to vestibular stimulation have been found in additional cortical areas, often concurrently with visual motion signals, such as in the frontal eye fields (Fukushima et al. 2000), the ventral intraparietal area (Bremmer et al. 2002; Schlack et al. 2002; Klam and Graf 2003), and the medial superior temporal area (Duffy 1998; Page and Duffy 2003; Gu et al. 2006, 2007; Takahashi et al. 2007; Liu and Angelaki 2009).

In the early 1990s, an additional vestibular-related area located deep in the sylvian (lateral) sulcus, in close proximity to the secondary somatosensory area (S2) and auditory area, was described in Java and squirrel monkeys (Grüsser et al. 1982, 1990; Guldin et al. 1992). The area was called the parietoinsular vestibular cortex (PIVC), where neurons were shown to respond to motion in darkness, as well as to optokinetic and proprioceptive/somatosensory stimulation (Grüsser et al. 1990; Guldin et al. 1992). Although little is known about the functional significance for the presence of vestibular signals in multiple cortical areas, the PIVC, which receives direct vestibular signals through the thalamus (Akbarian et al. 1992), has been described often as the "vestibular cortex" (Fukushima 1997; Guldin and Grüsser 1998).

PIVC has recently been identified in the retroinsular area (Ri) of rhesus macaques, bordering with and slightly overlapping with the S2 (Chen et al. 2010). Using smooth transient displacements in 3 dimensions, PIVC neurons were shown to modulate during rotation and/or translation in darkness but were not sensitive to optic flow. However, sinusoidal stimuli at multiple frequencies have been used traditionally to characterize the response properties of subcortical neurons (Dickman and Angelaki 2002; Angelaki et al. 2004; Shaikh, Ghasia, et al. 2005; Shaikh, Green, et al. 2005; Chen-Huang and Peterson 2006; Yakushin et al. 2006; Zhou et al. 2006). As a result, it is presently unknown how PIVC responses compare with those of subcortical neurons. Thus, the goal of the current report was to characterize PIVC response properties during rotation, translation, and combination stimuli, such that direct comparisons could be made with vestibular neurons in the thalamus (Meng et al. 2007; Marlinski and McCrea 2008), cerebellum (Shaikh, Ghasia, et al. 2005; Shaikh, Green, et al. 2005; Yakusheva et al. 2007, 2008), and vestibular nuclei (VN) (Angelaki and Dickman 2000; Dickman and Angelaki 2002, 2004; Angelaki et al. 2004). Such comparison is important to obtain a basic understanding of how vestibular information has been processed in cortical, as compared with subcortical, areas.

Materials and Methods

Subjects and Setup

Single-unit recordings were obtained from 3 hemispheres in 2 rhesus monkeys (*Macaca mulatta*) weighing between 6 and 10 kg. In a sterile surgical procedure, a circular delrin ring was chronically implanted to restrain and stabilize the head during experiments. Stainless steel inverted T-bolts and dental acrylic were used to attach the implant to the skull (for details, see Angelaki and Dickman 2000; Meng et al. 2005; Gu et al. 2006). All experiments and surgical operations were conducted according to the National Institutes of Health Guidelines

and were approved by the Animal Care and Use committee of Washington University.

During experiments, the monkeys were seated in a primate chair secured rigidly inside a vestibular turntable consisting of a 3-axis rotator mounted on top of a linear sled (Acutronics). This system could deliver pitch and roll rotation stimuli about an earth horizontal axis, yaw rotation stimuli about an earth vertical axis, as well as translational motion stimuli along any direction in the horizontal plane. Stimulus presentation and data acquisition were controlled with custom-written scripts within the Spike2 software environment using the Cambridge Electronics Device (CED, model power 1401) data acquisition system.

Neural Recordings

We recorded extracellularly the activities of single neurons in area PIVC using epoxy-coated tungsten microelectrodes (FHC, 1–2 MΩ impedance at 1 kHz). Electrodes were inserted into 26-gauge transdural guide tubes and advanced by a remote-controlled microdrive. Neural activities were amplified, filtered (0 Hz–10 kHz, notched at 60 Hz), and passed through a dual time–amplitude window discriminator (BAK Electronics). Single units were identified using consistent properties in wave shape, latency, and amplitude. Discriminated spikes were stored on PC through the event channel of CED power 1401 for off-line analyses.

Area PIVC was identified using magnetic resonance imaging scans (for details, see Chen et al. 2010). Data were collected from the same animals as those used by Chen et al. (2010) after the entire region of PIVC was mapped. The location of PIVC cells recorded in these experiments have been superimposed on flattened maps and coronal sections for the right hemispheres of each of the 2 animals, as illustrated in Figure 1. Recording locations were restricted to anterior regions of Ri, in the upper bank, and tip of the lateral sulcus (vestibular cells in the lower bank are less tuned and often have a significant second harmonic; see Chen et al. 2010; thus, the lower bank was not explored in the present experiments).

Experimental Protocols

As electrode penetrations extended into the PIVC area, the search stimulus consisted of 0.5 Hz sinusoidal translations and rotations about the cardinal axes (lateral and fore–aft for translation; yaw, pitch, and roll for rotation) in darkness. Upon cell isolation, the following motion protocols were delivered in complete darkness:

1. (1) A "classification" protocol consisted of 0.5 Hz (±20 cm, 0.2 G, G = 9.8 m/s^2) lateral and fore–aft translation stimuli, as well as 0.5 Hz (±10°) and 0.05 Hz (±30°) yaw, pitch, and roll rotation stimuli.
2. (2) For PIVC neurons that responded to translation, combinations of tilt and translation were delivered next. These stimuli were identical to those used previously to manipulate translational and net gravitoinertial accelerations (Angelaki et al. 2004; Meng et al. 2007; Yakusheva et al. 2007; Liu and Angelaki 2009). Specifically, they consisted of pure translation, pure tilt, or 2 combinations of translation and tilt: tilt – translation and tilt + translation. Importantly, the tilt stimulus consisted of a 0.5-Hz sinusoidal rotation from an upright position with peak amplitude of 11.3° (36°/s). Since this motion reorients the head relative to gravity, otolith afferents were stimulated by a linear acceleration component in the horizontal plane with a peak magnitude of 0.2 G. The amplitude of the translation stimulus was matched to that induced by the head tilt (0.2 G, ±20 cm). During combined tilt and translation, the translational and gravitational accelerations combined in either an additive or a subtractive manner, depending on the relative phase of the 2 stimuli. As a result, the net gravitoinertial acceleration in the horizontal plane either doubled (tilt + translation) or was nearly zero (tilt – translation), even though the actual translation remained the same. Each cell was tested at 2 orientations ($\theta = 0°$ and $\theta = 90°$) corresponding to lateral motion/roll tilt and fore–aft motion/pitch tilt, respectively.
3. (3) Translation-sensitive cells were also tested during lateral and fore–aft motion at different frequencies: 0.16 Hz (±0.1 G), 0.3 Hz (±0.1 G), 1 Hz (±0.2 G), 2 Hz (±0.3 G), and 5 Hz (±0.3 G). Translational motion activates only otolith (but not semicircular canal) vestibular afferents.
4. (4) For PIVC neurons that responded to yaw rotation, response dynamics were examined using different frequencies, including the following: 0.01 Hz (31.4°/s, ±500°), 0.02 Hz (31.4°/s, ±250°), 0.05 Hz (31.4°/s, ±100°), 0.1 Hz (31.4°/s, ±50°), 0.25 Hz (31.4°/s, ±20°), 1 Hz (31.4°/s, ±5°), and 2 Hz (15.1°/s, ±1.2°). Yaw rotation activates only semicircular canal (but not otolith) vestibular afferents.
5. (5) Rotation-sensitive cells were also tested during pitch and/or roll oscillations at different frequencies, including the following: 2 Hz (±1.2°), 1 Hz (±5°), 0.25 Hz (±22.6°), 0.1 Hz (±30°), 0.05 Hz (±30°), and 0.02 Hz (±30°). Roll and pitch rotations activate both semicircular canal and otolith vestibular afferents.

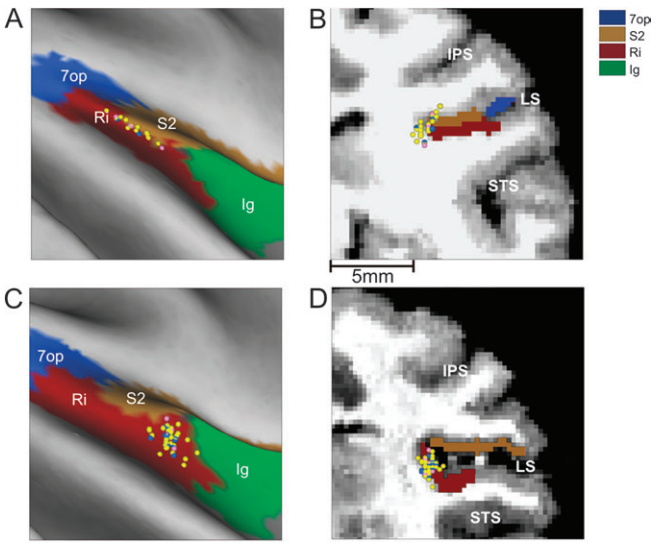

Figure 1. Magnetic resonance imaging–based reconstruction of recording locations. (*A*, *C*) Flat maps of the brain areas (color coded) around the lateral sulcus of the right hemisphere of monkey U (*A*) and the right hemisphere of monkey J (*C*), with cell locations mapped onto the surface. (*B*, *D*) Corresponding coronal sections with the 3 major sulci (IPS, LS, and STS) identified. Each dot corresponds to a cell responsive to vestibular stimulation ($n = 93$), color coded as follows: convergent ($n = 62$, yellow), translation only (17, blue), and rotation only ($n = 14$, pink). 7op, area 7 operculum; Ig, granular insula; IPS, intraparietal sulcus; LS, lateral sulcus; Ri, retroinsular area; S2, secondary somatosensory area; STS, superior temporal sulcus.

Data Analyses

Quantitative data analyses were performed off-line using custom-written scripts in Matlab (MathWorks). We first determined whether the cell modulated significantly at the first or second harmonic of each sinusoidal stimulus. For this, firing rates from multiple cycles (minimum of 10 cycles for frequencies larger than 0.1 Hz and minimum of 3 cycles for lower frequencies) were averaged and binned (40 bins per cycle), and then a fast Fourier transform was applied, obtaining the magnitude of the first 20 harmonics of each response. Two Fourier ratios were then computed, which were defined as the first harmonic (f1) or the second harmonic (f2), respectively, over the maximum of the remaining harmonics. Subsequently, the 40 response bins were shuffled randomly, and the 2 Fourier ratios were computed from the randomly permuted histograms, and this process was repeated 1000 times. If the Fourier ratio of the original data exceeded that for 99% of the permuted data sets, we considered the temporal modulation to be statistically significant ($P < 0.01$). Thus, for each stimulus, we computed 2 P values, P_f1 and P_f2, corresponding to the significance level for first and second harmonic modulations, respectively. Note that this analysis was necessary to identify first harmonic-responding cells (many cells in the lateral sulcus respond to the second harmonic; Chen et al. 2010). Only responses from first harmonic cells have been further considered in the present analysis (Table 1).

For responses that passed this modulation criterion, instantaneous firing rates (computed as the inverse of interspike interval and assigned

to the middle of the interval) from multiple cycles were stacked into a single cycle by overlaying the response to each cycle. The overlaid single-cycle responses were then fit with the sum of 2 sinusoids (first and second harmonics of the stimulus frequency) plus a constant term using a nonlinear least-squares minimization algorithm (Levenberg–Marquardt). Response amplitude refers to half the peak-to-trough modulation based on the first harmonic fit. For translational stimuli, neural gain was calculated as the response amplitude divided by the peak linear acceleration (spikes per second per G). Phase was expressed as the difference (degree) between peak response and peak linear acceleration. For rotational stimuli, neural response gain was computed as the ratio of response amplitude and peak angular head velocity (spikes per second per degree per second). Phase was expressed as the difference (degree) between peak response and peak head velocity.

The neural gain and phase during 2 motion directions in the horizontal plane were fitted by a 2D spatiotemporal convergence model (STC; Angelaki 1991, 1992). The STC model represents a generalization to cosine tuning, where neurons are allowed to have not just 1 but 2 response axes. As a result, response gain does not necessarily follow a rectified cosine as a function of motion direction and response phase could vary dependent upon stimulus direction. The larger the observed response to an orthogonal second axis the greater is the STC behavior. STC has been shown to occur for a small subpopulation of neurons in the fastigial and VN (Angelaki and Dickman 2000; Shaikh, Ghasia, et al. 2005; Chen-Huang and Peterson 2006). Four parameters for each cell were computed, including the preferred (maximum response) direction, the corresponding gain and phase along that direction, and the tuning ratio (i.e., ratio of minimum over maximum neural response gain).

To characterize response dynamics, we plotted gain and phase as a function of frequency. For translation response dynamics, we used gain and phase along the preferred (maximum response) direction, as computed from the STC model fits. For tilt response dynamics, we used gain and phase along any axis (pitch or roll), whichever produced the largest modulation. To compute averages and compare with response dynamics of cells in other brain areas, response gains were first normalized by dividing the gain at each frequency with the cell's gain measured at 0.5 Hz. This normalization was necessary to preserve the gain dependence on frequency, as not all cells were tested at all frequencies (but all were tested at 0.5 Hz), and neural response gain varied from cell to cell.

To determine whether the response modulation of each neuron correlated best with translation or net linear acceleration, linear regression analysis was used to simultaneously fit the cumulative cycles of cell modulation during each of the translation, tilt, and combined stimuli using "net acceleration–" and "translation"-coding models. Each of these models assumes that neuronal modulation is attributable either to the net acceleration or to the translation acceleration component (for details, see Angelaki et al. 2004; Green et al. 2005). To determine how well each of the models fitted the data, we computed partial correlation coefficients (corrected for the correlation between the 2 models), which were normalized using Fisher's r-to-z transform (Angelaki et al. 2004; Green et al. 2005).

Finally, to test whether a measured response distribution was uniform, a resampling analysis was adapted using the sum-squared error between the measured distribution and an ideal uniform distribution containing the same number of observations (for details, see Takahashi et al. 2007). For nonuniform distributions, we also performed a multimodality test based on the kernel density estimate method (for details, see Gu et al. 2006; Takahashi et al. 2007). This test generates 2 P values, with the first one (P_uni) for the test of unimodality and the second one (P_bi) for the test of bimodality. For example, if P_uni < 0.05 and P_bi > 0.05, unimodality is rejected and the distribution is classified as bimodal. If both P_uni and P_bi < 0.05, there are more than 2 modes in the distribution.

Results

We recorded from 146 well-isolated PIVC neurons that were either spontaneously active or responded to 0.5 Hz search motion stimuli in darkness (see Materials and methods). Most of the data were collected from the right hemispheres in 2 animals (76 and 47 cells, respectively), while the remaining 23 cells were recorded from the left hemisphere of one of the animals. Recording sites were concentrated in the upper bank and tip of the lateral sulcus, close to the anterior border between Ri and S2, as illustrated for the 2 right hemispheres in Figure 1.

As shown in Tables 1 and 2, a little more than half of the recorded cells were significantly modulated at the first harmonic of the stimulus: 54% (79/146) during translation and 52% (76/146) during rotation. Of these 93 cells that have been further considered in the present analysis, 62 neurons were "convergent" responding to both rotation and translation. Typical responses from an example convergent PIVC cell that modulated significantly (P_f1 ≤ 0.01 and P_f2 > 0.01) for all directions of rotation and translation are shown in Figure 2. The example cell exhibited the largest response during lateral translation, with a modulation gain of 207 spikes/s/G (Fig. 2*D*). Response gain was lower during fore–aft translation (161 spikes/s/G, Fig. 2*E*), and rotational gains were 0.4, 0.6, and 0.7 spikes/s/°/s for yaw (Fig. 2*A*), pitch (Fig. 2*B*), and roll (Fig. 2*C*), respectively. Next we summarize these properties, first for translation-responsive and then for rotation-responsive PIVC cells.

PIVC Responses during Translation

The preferred direction of PIVC neurons (convergent and nonconvergent) during translation was computed from each cell's responses during lateral and fore–aft motion using a 2D STC model (Angelaki 1991). The same STC model has previously been used to describe otolith-driven responses in central vestibular neurons (Angelaki and Dickman 2000; Shaikh, Ghasia, et al. 2005; Chen-Huang and Peterson 2006). Figure 3*A* illustrates a polar plot, summarizing the maximum response direction and gain for each of the 79 PIVC neurons responsive to 0.5 Hz translation. The maximum response directions were broadly and uniformly distributed within the horizontal plane (uniformity test, P = 0.8), with maximum response gains averaging (±standard error of the mean [SEM]) 303.2 ± 20.6 spikes/s/G (range 26.2–1145.7 spikes/s/G). There was no difference in either gain or preferred direction for convergent versus nonconvergent cells (Wilcoxon rank test, gain: P = 0.13; preferred direction: P = 0.65; Fig. 3*A*, filled vs. open symbols, respectively). Note that leftward and rightward preferred directions (polar angles of 180° and 0°, respectively)

Table 1
Statistics of response modulation during sinusoidal translation (0.5 Hz)

	Left–right	Fore–aft	Maximum direction
P_f1 ≤ 0.01 and P_f2 > 0.01	57 (39%)	59 (40%)	79 (54%)
P_f2 ≤ 0.01	10 (7%)	8 (6%)	11 (8%)
Unresponsive P_f1 and P_f2 > 0.01	79 (54%)	79 (54%)	56 (38%)

Table 2
Statistics of response modulation during sinusoidal rotation (0.5 Hz)

	Yaw	Pitch	Roll	Maximum direction
P_f1 ≤ 0.01 and P_f2 > 0.01	29 (20%)	49 (34%)	43 (30%)	76 (52%)
P_f2 ≤ 0.01	4 (3%)	6 (4%)	6 (3%)	12 (8%)
Unresponsive P_f1 and P_f2 > 0.01	113 (77%)	91 (62%)	98 (67%)	59 (40%)

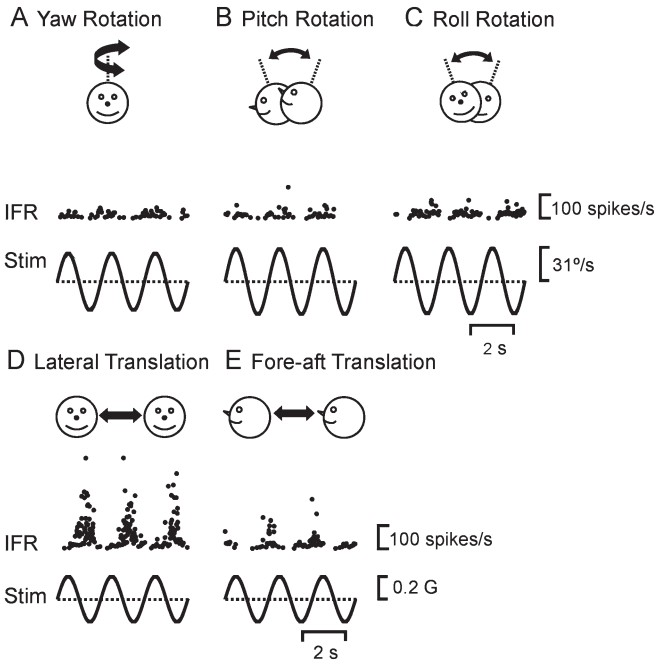

Figure 2. Example PIVC neuron responses during (*A*) yaw rotation, (*B*) pitch rotation, (*C*) roll rotation, (*D*) lateral translation, and (*E*) fore–aft translation (0.5 Hz). IFR, instantaneous firing rate; Stim, head angular velocity (*A*, *B*, C) or linear acceleration (*D* and *E*); sp, spikes; G = 9.8 m/s^2.

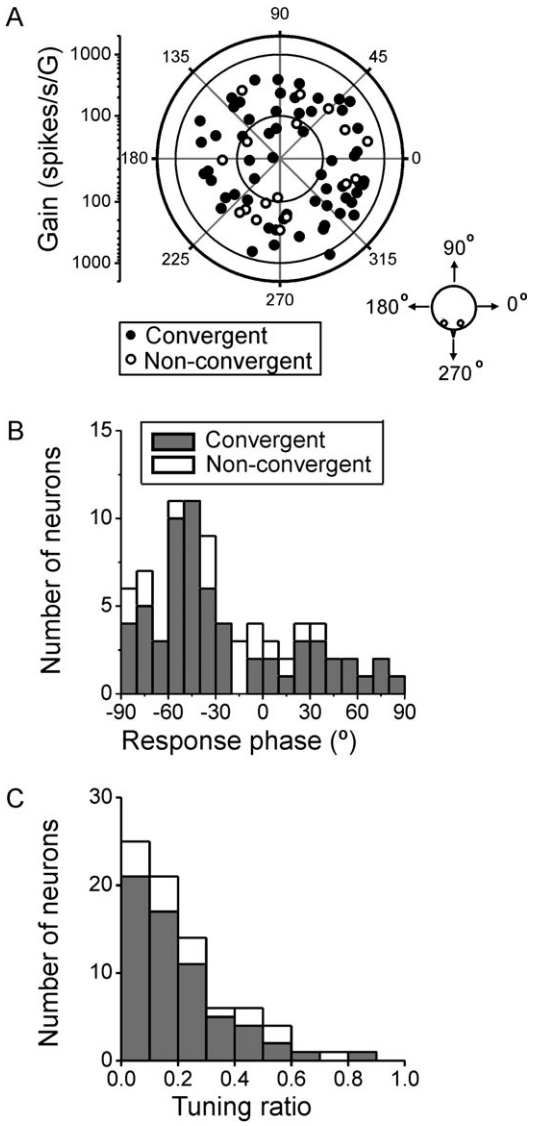

Figure 3. Distributions of preferred direction, gain, and phase. (*A*) Polar plot of maximum response direction and gain during translation (0.5 Hz). Each data point corresponds to a cell (n = 79). The distance of each data point from the center corresponds to the neuron's response gain (in units of spikes per second per G, G = 9.81 m/s^2), whereas its polar angle illustrates the cell's preferred direction in the horizontal plane (see cartoon). Filled circles: convergent neurons (n = 62); open circles: nonconvergent neurons (n = 17). (*B*) Distribution of response phase (computed for the preferred direction). A phase of 0° illustrates responses in phase with acceleration. (*C*) Distribution of tuning ratio, computed as the ratio of the gains along the preferred and orthogonal response directions. Filled versus open bars illustrate convergent (i.e., responding to both rotation and translation) and nonconvergent (i.e., sensitive only to translation) neurons, respectively.

are similarly distributed. Thus, because most of these cells were recorded from the right hemisphere, there appears to be little lateralization of the translation preferred directions in PIVC neurons.

Figure 3*B* shows the distribution of response phase along the preferred translation direction in the horizontal plane. The distribution was not uniform (uniformity test, $P < 0.001$) but instead unimodal ($P_{\_uni} = 0.51$, modality test). Most cells lagged (negative phase values of 30–60°) linear acceleration, and there was no difference in response phase for convergent and nonconvergent cells (Wilcoxon rank test, $P = 0.7$; Fig. 3*B*, filled vs. open symbols, respectively). The distribution of tuning ratios (i.e., the ratio of minimum over maximum response gains in the horizontal plane) was not uniform (uniformity test, $P < 0.001$) but unimodal ($P_{\_uni} = 0.27$, modality test), with most neurons having tuning ratios <0.3 (Fig. 3*C*). Small tuning ratios indicate cosine spatial tuning with little response to translational motion in directions orthogonal to the maximum response direction (little STC). Large tuning ratios indicate broad tuning to all spatial directions of translational motion in the horizontal plane (strong STC). There was no difference in tuning ratio for convergent and nonconvergent cells (Wilcoxon rank test, $P = 0.15$). These response properties of PIVC neurons during 0.5-Hz translation are similar to those of neurons in the thalamus (Meng et al. 2007), VN/cerebellar nuclei (CN) (Angelaki and Dickman 2000; Dickman and Angelaki 2002; Shaikh, Ghasia, et al. 2005), and also the dorsal medial superior temporal area (MSTd) (Liu and Angelaki 2009).

PIVC Responses during Combinations of Tilt and Translation

Primary otolith afferents, due to the properties of mechanosensory transduction and the laws of physics (Angelaki et al. 2004), cannot distinguish between translational acceleration and tilts of the head relative to gravity. Instead, otolith afferents exhibit firing rates that are proportional to net linear acceleration (i.e., the sum of inertial acceleration and gravity; Fernández and Goldberg 1972; Si et al. 1997; Angelaki et al. 2004). However, it has been shown that central vestibular and cerebellar neurons utilize signals from both the otolith and semicircular canal afferents to distinguish translational motion from head tilt (Angelaki et al. 2004; Yakusheva et al. 2007). To investigate whether PIVC neurons encode translation, tilt, or net linear acceleration, responses were obtained using translation, tilt, or combined translation and tilt at 2

orientations (θ = 0° and θ = 90°). The combined translation/tilt motions corresponded to lateral motion/roll tilt and fore–aft motion/pitch tilt, respectively (see Materials and methods and Angelaki et al. 2004; Yakusheva et al. 2007; Liu and Angelaki 2009). As shown in Figure 4, the translation and tilt stimulus amplitudes were "matched," such that the horizontal linear acceleration components were equivalent (0.2 G). Thus, during the combination stimuli, the horizontal net acceleration was either zero (tilt – translation) or doubled (0.4 G, tilt + translation).

The example cell in Figure 4 responded during fore–aft motion (θ = 90°, Fig. 4*A*, top row) but did not modulate during lateral motion (θ = 0°, Fig. 4*A*, second row). In addition, the neuron was not responsive to head tilt, even though the net linear acceleration was the same (Fig. 4*A*,*B*, bottom row). Importantly, response modulation amplitudes during tilt – translation (Fig. 4*C*) and tilt + translation (Fig. 4*D*) were similar to those observed during translation only (Fig. 4*A*). Specifically, whenever a head tilt to the right occurred simultaneously with translation to the left, gravitational and inertial accelerations were oppositely directed and canceled (tilt – translation). In this case, net acceleration is zero, and otolith afferents cease to modulate (Angelaki et al. 2004). In contrast, whenever a head tilt to the right occurred simultaneously with translation to the right, the accelerations summed, resulting in net linear acceleration that was double that for each movement alone (tilt + translation).

Regardless of the stimulus, the cell's firing rate followed the translation stimulus and was relatively unresponsive to changes in head orientation relative to gravity. This occurs whenever central vestibular neurons receive, in addition to otolith information, signals from the semicircular canals. Importantly, this otolith/canal convergence must be spatially and temporally matched, as previously shown for cerebellar neurons (Yakusheva et al. 2007, 2008). Note that, in addition to response amplitude, the modulation phase during translation and tilt – translation was similar; both were ~180° different from the phase during tilt + translation. This is because the translation and tilt stimulus phases are inverted for tilt + translation and tilt – translation (compare Fig. 4*C*,*D*, second and third rows from bottom).

These response characteristics are shown for all PIVC cells in Figure 5, which plots peak modulation amplitude and phase during the tilt, tilt – translation, and tilt + translation stimuli as a function of the respective translation response. Dotted blue and solid red lines illustrate the predictions of coding for net acceleration and translation, respectively. Most PIVC neuron responses followed the translational acceleration, similar to the example neuron of Figure 4. In fact, most PIVC neuron tilt responses were significantly attenuated as compared with their translation responses (Wilcoxon rank test, $P << 0.001$; Fig. 5*A*). In addition, tilt – translation and tilt + translation modulation amplitudes were essentially equivalent to those obtained during translation-only stimulation (Fig. 5*B*,*C*, respectively; Wilcoxon rank test, $P = 0.7$, $P = 0.3$), and regression fits to the amplitude plots had slopes that were not different from unity (tilt – translation vs. translation: 1.07, 95% confidence interval [CI] = [0.96, 1.18], $r = 0.8$, $P < 0.001$; tilt + translation vs. translation: 0.94, 95% CI = [0.83, 1.05], $r = 0.7$, $P < 0.001$). In addition to response amplitude, response phase also followed the translation predictions (Fig. 5*D*–*F*), including a 180° phase reversal during tilt + translation (see also Fig. 4).

These results have been further quantified by computing partial correlation coefficients that describe how well each cell's responses to all 4 stimuli (translation, tilt, tilt – translation, and tilt + translation) were simultaneously fitted by translation-coding (Fig. 4, third row from bottom) and net acceleration–coding (Fig. 4, bottom row) models. These partial correlation coefficients were normalized using Fisher's *r*-to-*z* transform (Angelaki et al. 2004) and plotted as shown in Figure 6. Normalization allows a visual inspection of how well each cell's response followed the predictions (translation or net

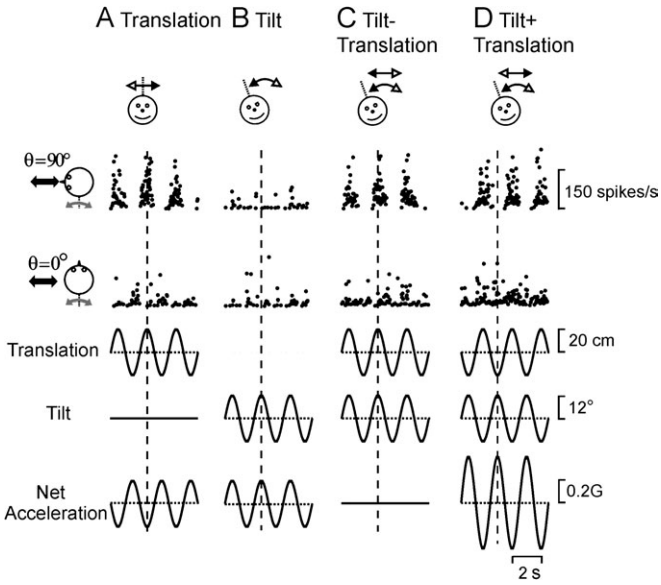

Figure 4. Example PIVC neuron responses during combinations of tilt and translation. (*A*) Translation only, (*B*) tilt only, (*C*) tilt − translation, and (*D*) tilt + translation (0.5 Hz). Data are shown along 2 stimulation axes (cartoon drawings), with the translation/tilt position (bottom traces) being matched in both amplitude and direction to elicit an identical net acceleration in the horizontal plane. Vertical dotted lines mark the times of peak stimulus amplitude.

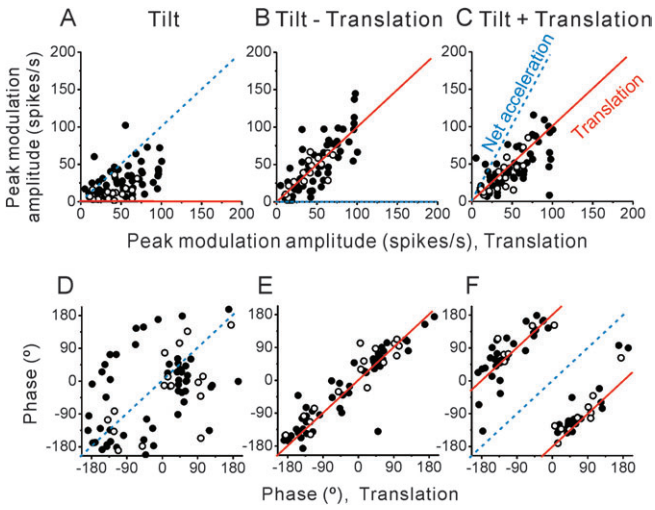

Figure 5. Summary of tilt/translation responses. Peak response amplitude and phase during (*A*, *D*) tilt, (*B*, *E*) tilt − translation, and (*C*, *F*) tilt + translation are plotted as a function of the corresponding response during translation (0.5 Hz, $n = 71$). Filled symbols: convergent neurons; open symbols: nonconvergent neurons. Solid red lines indicate the predictions when cells selectively encode translation, whereas dashed blue lines illustrate the predictions of encoding net linear acceleration.

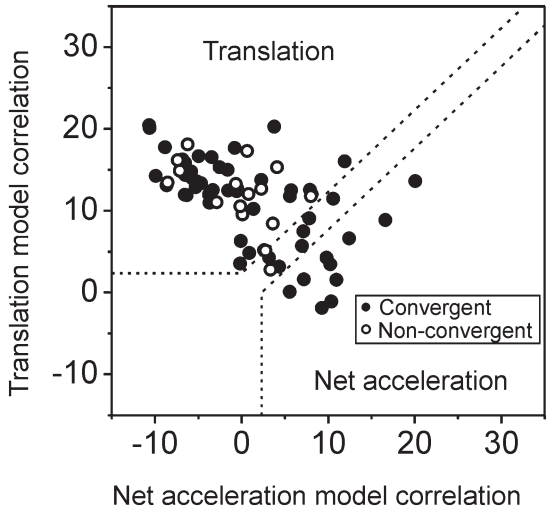

Figure 6. Summary of tilt/translation responses. Scatter plot of *z*-transformed partial correlation coefficients for fits of each cell responses with translation and net acceleration-coding models ($n = 71$). The superimposed dashed lines divide the plot into 3 regions: an upper/left area corresponding to cell responses that were significantly better fit ($P < 0.01$) by the translation-coding model; a lower/right area that includes neurons that were significantly better fit by the net acceleration model; and an in-between area that would include cells that were not significantly better fit by either model. Filled symbols: convergent neurons; open symbols: nonconvergent neurons.

acceleration), with dotted lines marking the 0.01 level of significance. Seventy-six percentage of PIVC neurons (54/71) fell in the upper left quadrant, reflecting the fact that their firing rates were better correlated with the translation stimulus. In contrast, only 14% (10/71), all of which were convergent cells (Fig. 6, filled symbols), exhibited responses that were better correlated with the net acceleration stimulus.

Response Dynamics: Translation

Twenty-six PIVC neurons that responded during translation and whose isolation was maintained after completion of the tilt/translation protocol were further tested at different frequencies, as illustrated with the firing rates of an example PIVC neuron during lateral ($\theta = 0°$) and fore–aft ($\theta = 90°$) motion in Figure 7*A*. The gain and phase responses to the 2 stimulus directions were fitted by the STC model (see Materials and methods). For each frequency, gain and phase were thus computed along the preferred direction in the horizontal plane. These data are summarized separately for each cell (gray) and as mean responses (black) in Figure 7*B,C*. The translation gains decreased with increasing frequency (Fig. 7*B*; analysis of covariance [ANCOVA], $F_{1,113} = 32.5$, $P < 0.001$), with a slope of –0.33 (CI = [–0.44, –0.21], $r = -0.47$, $P < 0.001$). Flat acceleration gains as a function of frequency are indicative of responses that follow linear acceleration, whereas acceleration gains that decrease with unity slope are indicative of responses that follow linear velocity. The value of 0.33 for the mean gain slope (Fig. 7*B*) suggests that, on average, PIVC translation responses carry information about both linear acceleration (mostly) and linear velocity. Certainly, individual PIVC neurons vary in their response dynamics, some encoding closer to acceleration (flat slope) and some closer to head velocity (steep slope). Response phase showed no dependence on frequency (Fig. 7*C*; ANCOVA, $F_{1,113} = 1.06$, $P = 0.3$).

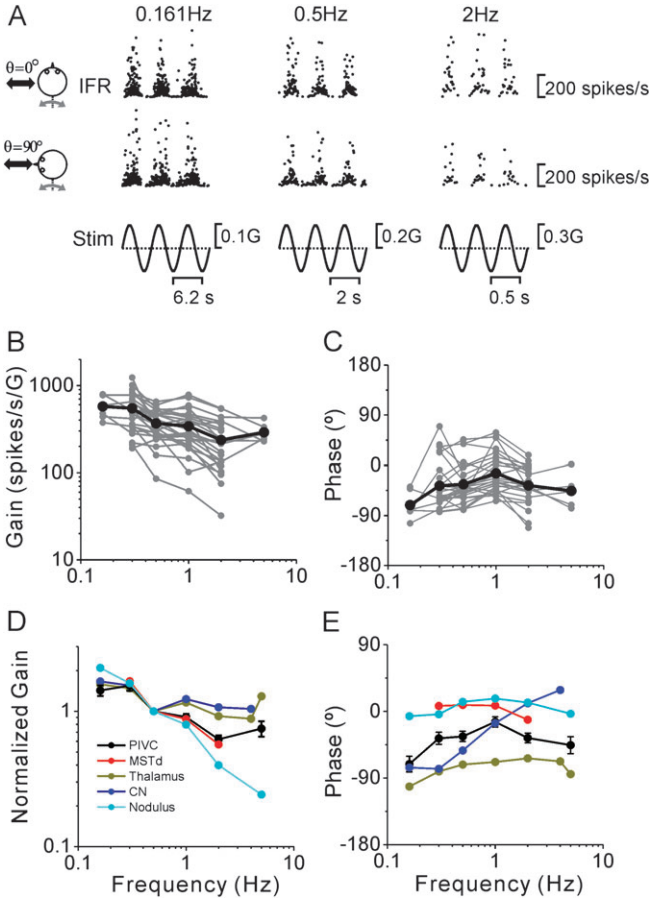

Figure 7. Summary of PIVC cell dynamics during translation. (*A*) Instantaneous firing rate (IFR) of an example PIVC cell during lateral and fore–aft translation at 0.161, 0.5, and 2 Hz. (*B*, *C*) Response gain and phase (expressed relative to linear acceleration and computed along the preferred direction) of each PIVC cell ($n = 26$; gray symbols and lines) are plotted versus frequency. Black thick lines and symbols illustrate the population averages. (*D*, *E*) Mean normalized gain and phase (±standard deviation) of PIVC neurons (black) are compared with the corresponding data from MSTd (red; replotted with permission from Liu and Angelaki 2009), thalamus (dark yellow; replotted with permission from Meng et al. 2007), CN (blue; replotted with permission from Shaikh, Ghasia, et al. 2005), and simple spikes of nodulus/uvula Purkinje cells (cyan; replotted with permission from Yakusheva et al. 2008).

To compare the response dynamics of PIVC neurons with those of cells in other brain areas, mean gain (normalized to unity at 0.5 Hz) and phase values (±SEM) have been superimposed in Figure 7*D,E* with corresponding data from MSTd (Liu and Angelaki 2009; red), thalamus (Meng et al. 2007; green), CN (Shaikh, Ghasia, et al. 2005; blue), and nodulus/uvula Purkinje cells (Yakusheva et al. 2008; cyan) shown. The frequency dependence of the gain in PIVC neurons differed from the frequency dependence of subcortical neurons (ANCOVA, $P < 0.001$). Specifically, in PIVC, the gain decrease with frequency was steeper than in the thalamus and CN but shallower than in the nodulus/uvula. Note that, although the difference between PIVC and MSTd dynamics was marginally significant (ANCOVA, $F_{1,260} = 4$, $P = 0.05$), this comparison was only based on a limited frequency range, since MSTd cells were not tested at frequencies greater than 2 Hz (Fig. 7*D*, red).

We did not perform statistical comparisons for response phase since, similar to other translation-sensitive neurons, the phase of PIVC cells varied greatly for individual neurons

(Fig. 7*C*, see also Fig. 3*B*). Such a distributed phase representation of otolith-driven signals is commonly observed both in the thalamus (Meng et al. 2007) and in the VN and deep CN (Angelaki and Dickman 2000; Dickman and Angelaki 2002; Shaikh, Ghasia, et al. 2005). Still, across the PIVC population of cells tested, phase remained relatively constant with frequency, a finding which is consistent with neurons in MSTd (red; Liu and Angelaki 2009), thalamus (green; Meng et al. 2007), and nodulus/uvula (cyan; Yakusheva et al. 2008) but differs from neurons in CN (blue; Shaikh, Ghasia, et al. 2005) and VN (Angelaki and Dickman 2000; Dickman and Angelaki 2002), where sharp phase changes with frequency are often observed (Fig. 7*E*; note that VN data are not plotted because mean responses were not reported in previous publications).

Response Dynamics: Rotation

Twenty-nine (20%) PIVC neurons (26/29 were convergent) also modulated significantly during yaw rotation (Table 2). Of these, 12 neurons (41.4%) were type I (i.e., firing rate increased during ipsilateral rotation) and 17 neurons (58.6%) were type II (i.e., firing rate increased during contralateral rotation). PIVC neuron response dynamics were examined across the frequency range from 0.01 to 2 Hz, as shown in Figure 8*A*–*C*. In general, yaw response gains (re head velocity) increased with frequency (ANCOVA, $F_{1,77} = 33$, $P < 0.001$), with a mean slope of 0.25 (CI = [0.16, 0.34], $r = 0.54$, $P < 0.001$) (Fig. 8*B*), whereas response phase was independent of frequency (Fig. 8*C*; ANCOVA, $F_{1,77} = 0.13$, $P = 0.7$). As illustrated in Figure 8*D*,*E*, yaw response dynamics in PIVC were similar to those of non-eye movement VN neurons ($F_{1,193} = 1$, $P = 0.3$; data from Dickman and Angelaki 2004; see also Waespe and Henn 1977) and thalamic cells ($F_{1,177} = 3.2$, $P = 0.07$; data from Meng et al. 2007; see also Büttner et al. 1977). Note that nodulus/uvula Purkinje cells do not respond to yaw rotation (Yakusheva et al. 2008, 2010) and that CN and MSTd response dynamics during yaw are not yet available.

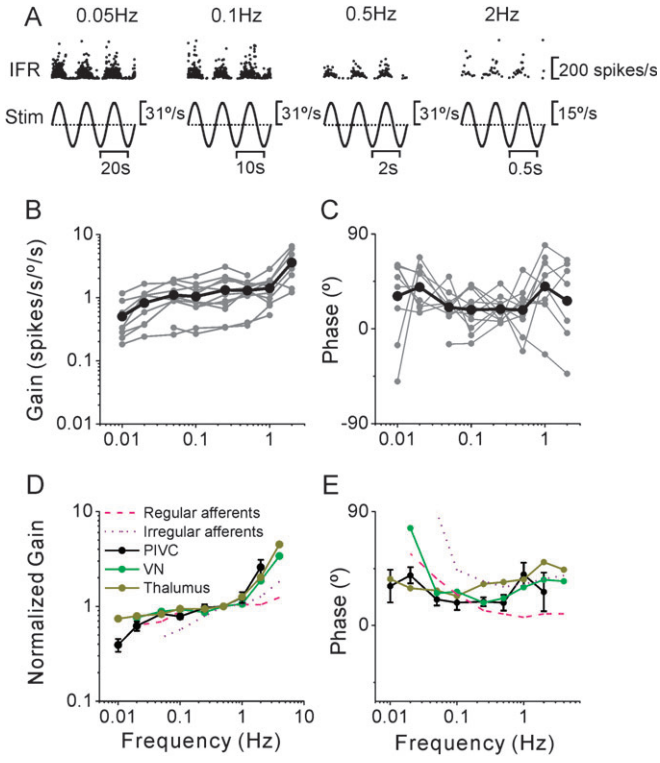

Figure 8. Summary of PIVC cell dynamics during yaw rotation. (*A*) Instantaneous firing rate (IFR) of an example PIVC cell during yaw rotation at 0.05, 0.1, 0.5, and 2 Hz. (*B*, *C*) Response gain and phase (expressed relative to angular velocity) of each PIVC cell ($n = 11$; gray symbols and lines) are plotted versus frequency. Black thick lines/symbols illustrate population averages. (*D*, *E*) Mean normalized gain and phase (±standard deviation) of PIVC neurons (black) are compared with the corresponding data from the VN (green; replotted with permission from Dickman and Angelaki 2004) and thalamus (dark yellow; replotted with permission from Meng et al. 2007). Data from regular and irregular canal afferents are also shown for comparison (red dashed and dotted lines; replotted with permission from Haque et al. 2004).

However, PIVC response dynamics differed from those of vestibular afferents (Fig. 8*D*,*E*, dashed and dotted lines show data from Haque et al. 2004), in both gain and phase. As shown previously, central vestibular neurons, including those in PIVC, exhibit a shallower decrease in yaw response gain as frequency decreases below ~0.1 Hz and a steeper gain increase as frequency increases above 1 Hz than do vestibular afferents. Differences in response phase were also observed. At high frequencies, central neurons are characterized by phase leads, similar to irregular firing canal afferents (Fig. 8*E*, dotted line). But the steeply increasing phase leads with decreasing frequency, characterizing canal afferents (Goldberg and Fernandez 1971; Haque et al. 2004), were absent from the dynamics of central neurons, including PIVC, where phase remains relatively constant across frequency. These low-frequency gain and phase differences between canal afferents and central neurons reflect the influences of "velocity storage" (Raphan et al. 1979; see Discussion).

The dynamics of PIVC neurons to pitch and/or roll tilt, stimuli that activate both semicircular canal and otolith afferents, exhibited more variance than the responses to yaw rotation. Note that pitch and roll responses have been considered together here, for each cell showing either pitch or roll responses, whichever was the largest. As shown in Figure 9 for 2 PIVC neurons, some cells maintained a strong modulation at both low and high frequencies (Fig. 9*A*, top row; convergent neuron), whereas others had a strong response only at low frequencies (Fig. 9*A*, bottom row; nonconvergent neuron). This variability in high-frequency response gain has been summarized for all cells in Figure 9*B*,*C*, which plots gain and phase separately for convergent (gray lines) and nonconvergent cells (i.e., rotation-only cells, black lines). Across the population, the mean gain decreased with increasing frequency (ANCOVA, $F_{1,103} = 28$, $P < 0.001$), with a slope of –0.28 (CI = [–0.39, –0.17], $r = -0.45$, $P < 0.001$) (Fig. 9*B*). There was a significant difference in the mean gain dependence on frequency for convergent and nonconvergent neurons ($F_{1,102} = 7.5$, $P = 0.007$). Nonconvergent cells had gains that decreased with increasing frequency for the whole frequency range tested (Fig. 9*B*, black), whereas convergent cells exhibited U-shaped gains across the frequency bandwidth tested (Fig. 9*B*, gray). Convergent cells also had higher tilt gains than nonconvergent neurons ($F_{1,103} = 21$, $P < 0.001$). Tilt response phase increased with frequency (ANCOVA, $F_{1,103} = 15$, $P < 0.001$), and there was no significant difference between convergent and nonconvergent cells (ANCOVA, $F_{1,103} = 0.004$, $P = 0.94$; Fig. 9*C*).

How the gain and phase dependence on frequency in PIVC compares with that in the VN and nodulus/uvula is illustrated in Figure 9*D*,*E* (tilt response dynamics of MSTd, CN, and thalamus are not yet available). The frequency dependence of

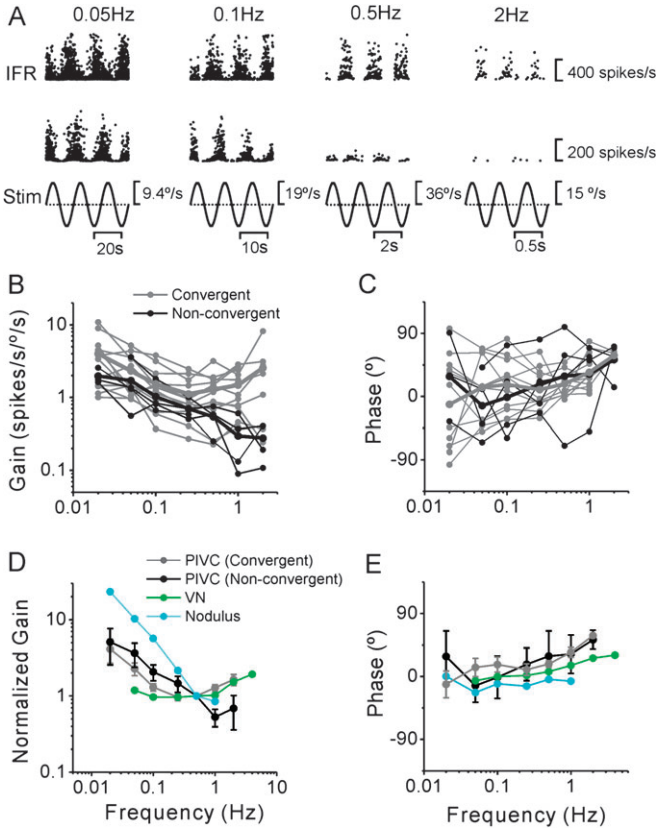

Figure 9. Summary of PIVC cell dynamics during tilt. (*A*) Instantaneous firing rate (IFR) of 2 example PIVC cells during tilt at 0.05, 0.1, 0.5, and 2 Hz. (*B*, *C*) Response gain and phase (expressed relative to angular velocity) of each PIVC cell ($n = 16$; gray: convergent cells; black: nonconvergent cells) are plotted versus frequency. (D, E) Mean normalized gain and phase (±standard deviation) of PIVC neurons (black) are compared with corresponding data from the VN (green; replotted with permission from Dickman and Angelaki 2004) and simple spikes of nodulus/uvula Purkinje cells (cyan; replotted with permission from Yakusheva et al. 2008).

tilt responses of both convergent and nonconvergent (i.e., rotation only) PIVC neurons differed from the gain dependence on frequency reported in Purkinje cell simple spike responses ($F_{1,206} = 51.1$, $P < 0.001$ and $F_{1,157} = 4.3$, $P = 0.04$, respectively; data from Yakusheva et al. 2008) and in VN canal–only neurons (Dickman and Angelaki 2004).

Discussion

In these experiments, we have compared the motion response properties of PIVC neurons with those in brain stem, cerebellum, and thalamus. The majority of PIVC neurons were convergent and modulated during both translation and rotation stimuli. Using combinations of translation and tilt movements, we also show that the firing rates of more than 3 quarters of PIVC neurons were better correlated with translation rather than net linear acceleration; only 14% of PIVC responses were better correlated with the net acceleration stimulus.

Response dynamics during yaw rotation were similar to those in vestibular-responding neurons in the brain stem and thalamus. In contrast, the dynamics during tilt and translation differed in many respects from those in subcortical neurons. Below we discuss these findings in relationship to previously published data in central vestibular areas.

Yaw Rotation Responses

To date, there have been only 2 other studies characterizing vestibular responses in PIVC (Grüsser et al. 1990; Chen et al. 2010). Grüsser et al. (1990) were the first to record from PIVC neurons in *Macaca fascicularis* monkeys during yaw, pitch, and roll rotation. They reported that some cells modulated during rotation about any axis, although quantitative data were presented only for yaw rotation (0.1–1 Hz). Here, we have characterized the dynamics during yaw rotation in a broader frequency range (0.01–2 Hz; Fig. 8). Response gains remained relatively flat between 0.1 and 1 Hz (the frequency range tested by Grüsser et al. 1990) but increased at 2 Hz and showed some decrease at 0.01 and 0.02 Hz. There was also a persistent phase lead of 20–40° at all frequencies relative to head velocity in our data sample. Thus, in general, our findings support and extend those by Grüsser et al. (1990).

Further, we observed that PIVC response dynamics to yaw rotations were similar to those reported for cells in the VN and thalamus but different from canal afferent dynamics (Fig. 8*D*,*E*). The absence of large low-frequency phase leads and gain decreases illustrate that PIVC yaw responses likely exhibit velocity storage properties, similarly as VN neurons (Buettner et al. 1978; Dickman and Angelaki 2004) and thalamus (Büttner et al. 1977; Meng et al. 2007; Marlinski and McCrea 2008). Thus, it is likely that PIVC responses show a much slower response decline as a function of time than canal afferents following rotational motion step inputs, as previously shown in the VN (Waespe and Henn 1977; Reisine and Raphan 1992). Velocity storage properties, that is, lengthening of the canal time constant and improvement in low-frequency coding of angular velocity, characterize both the vestibulo-ocular reflex (Cohen et al. 1977; Raphan et al. 1979) and rotational motion perception (Mergner et al. 1991; Howard et al. 1998; Okada et al. 1999).

The percentages of type I versus type II yaw responses reported here is similar to those described by Grüsser et al. (1990). However, we found that PIVC neurons had a much higher gain to rotational motion than Grüsser et al. (1990) reported. In our sample of yaw-responding neurons (20% of tested cells), the mean gain value at 0.5 Hz was 0.83 spikes/s/°/s, as compared with 0.11 spikes/s/°/s reported at 0.2 Hz by Grüsser et al. (1990) and 2.01 spikes/s/°/s in 8% of their sample tested at 0.5 Hz by Chen et al. (2010). The difference is likely due to different criteria for considering "responding" cells. For example, we used a statistical criterion to define significant response modulation (see Materials and methods and Chen et al. 2010), whereas Grüsser et al. (1990) considered all response gains >0.04 spikes/s/°/s as sensitive to yaw rotation; this can explain both the higher proportion of yaw-responding cells and the smaller average gain reported by Grüsser et al. (1990) as compared with our studies. Note also that the yaw stimulus used here was one and a half times stronger than that used by Chen et al. (2010); this difference can also explain the larger proportion of yaw-responding cells and the smaller average gain reported here as compared with those reported by Chen et al. (2010).

Collectively, mean yaw responses in PIVC are similar to those reported in the VN: for example, 0.77 spikes/s/°/s (Buettner et al. 1978) and 1.02 spikes/s/°/s (Dickman and Angelaki 2004), but larger than thalamus responses: 0.56 spikes/s/°/s (Büttner et al. 1977), 0.45 spikes/s/°/s (Marlinski

and McCrea 2008), and 0.5 spikes/s/°/s (Meng et al. 2007). Vestibular afferents generally have gains that are smaller than those observed in central neurons (Goldberg and Fernandez 1971; Haque et al. 2004; Ramachandran and Lisberger 2006; Sadeghi et al. 2007). It has been shown in a number of species that central vestibular neurons are more sensitive to rotational motion than are primary afferents, largely through commissural convergence of signals from the bilateral receptors (Shimazu and Precht 1965, 1966; Kasahara et al. 1968; Kasahara and Uchino 1974; Uchino et al. 1986; Malinvaud et al. 2010).

Translation Responses

Chen et al. (2010) also characterized PIVC neuron responses in rhesus macaques during 3D vestibular stimulation using stimuli consisting either of 0.5-Hz sinusoidal oscillations or of a smooth angular and linear displacement. Robust translation responses were reported in PIVC (Chen et al. 2010). In fact, similar to the present study, most neurons modulated during both rotation and translation. Responses were stronger in the upper bank and tip of the lateral sulcus, whereas weaker and often bidirectional (i.e., second harmonic) responses were observed in the lower bank of the lateral sulcus. Along the anterior–posterior dimension, vestibular responses were encountered throughout the whole extent of the Ri, at its border with S2 (Chen et al. 2010). In the present experiments, we did not survey the whole area explored by Chen et al. (2010). Our penetrations centered on the anterior Ri, close to the border with S2 (Fig. 1). Note that none of the vestibular response properties depended on location along the anterior/posterior dimension of the PIVC (Chen et al. 2010).

Using transient displacements with a biphasic acceleration profile, both velocity- and acceleration-like responses were reported in the macaque PIVC (Chen et al. 2010). In the current study, the decline of acceleration gains with increased frequency (Fig. 7) is in line with PIVC neurons encoding a combination of linear acceleration and linear velocity. In addition, preferred response directions of PIVC neurons were distributed throughout the horizontal plane, as shown previously for the thalamus (Meng et al. 2007), VN (Angelaki and Dickman 2000; Dickman and Angelaki 2002), and CN (Shaikh, Ghasia, et al. 2005).

Translation responses in PIVC were strong, averaging 303 spikes/s/G (preferred direction in the horizontal plane, 0.5 Hz). These gains are as large or larger than the mean translation response gains reported in MSTd (269 spikes/s/G; Liu and Angelaki 2009), CN (206 spikes/s/G; Shaikh, Ghasia, et al. 2005), and nodulus/uvula simple spike responses (305 spikes/s/G; Yakusheva et al. 2007, 2008) and substantially larger than those reported in the thalamus (Meng et al. 2007: 104 spikes/s/G; Marlinski and McCrea 2008: 111 spikes/s/G). Translation response gains in the VN were reported to average 219 spikes/s/G (convergent cells) and 134 spikes/s/G (nonconvergent cells) (Angelaki and Dickman 2000; Dickman and Angelaki 2002; Zhou et al. 2006). No such difference in translation response gain between convergent and nonconvergent neurons has been found in PIVC (Fig. 3*A*) and thalamus (Meng et al. 2007; Marlinski and McCrea 2008).

In contrast to robust translational modulation, none of the PIVC neurons in Java and squirrel monkeys responded to static tilt (Akbarian et al. 1988; Grüsser et al. 1990). This result could be relevant to our findings that most PIVC neurons encoded translational motion and not head tilt relative to gravity at 0.5 Hz (Fig. 5). Thus, the majority of PIVC neurons appear to discriminate translational from net gravitoinertial acceleration, similar to cells in area MSTd (Liu and Angelaki 2009) and the cerebellar nodulus and ventral uvula (Yakusheva et al. 2007, 2008, 2010). In contrast, vestibular responses in the thalamus, as well as in the VN and CN, reflect a continuum of coding translation and net linear acceleration (Angelaki et al. 2004; Meng et al. 2007).

Functional Roles of PIVC

Taken together, these studies begin to provide a description of the properties of PIVC neurons in response to motion. By using identical stimuli as those used to characterize subcortical vestibular responses, a direct comparison of their properties has been possible. But what do these findings tell us about the functional roles of PIVC? Unfortunately, our current understanding of the functional significance of these signals remains limited. Through the present study, we have gained a greater understanding of how PIVC neurons encode motion. In addition, we have gained insight as to how PIVC cells compare with other vestibular neurons in the brain stem, cerebellum, and thalamus. However, we have yet to understand how PIVC neurons perform during functionally relevant behavioral tasks such as movement detection or spatial motion discrimination. These answers await further study.

Moreover, the input/output connectivity of PIVC, information critical to its function, has yet to be quantified in detail. We do know that PIVC receives inputs from the ventral posterior areas in the thalamus that are known to respond to vestibular stimulation (Akbarian et al. 1992). We also know that PIVC is interconnected with other cortical areas that respond to head motion, including area 3a, area 2v, and the ventral posterior sylvian area that lies posterior to PIVC at the posterior tip of the lateral sulcus (Guldin et al. 1992). However, the functions of these areas also remain unknown. Finally, PIVC and the other interconnected cortical vestibular areas are known to project back to the VN (Akbarian et al. 1993, 1994; Nishiike et al. 2000), although the types of signals they convey and the types of VN neurons they project to have yet to be characterized in detail (but see Wilson et al. 1999). Much has yet to be learned about cortical vestibular processing and the functions that these diverse representations of vestibular information subserve.

Funding

National Eye Institute of the National Institutes of Health (EY017866).

Notes

Conflict of Interest: None declared.

References

Akbarian S, Berndl K, Grusser OJ, Guldin W, Pause M, Schreiter U. 1988. Responses of single neurons in the parietoinsular vestibular cortex of primates. Ann N Y Acad Sci. 545:187–202.

Akbarian S, Grusser OJ, Guldin WO. 1992. Thalamic connections of the vestibular cortical fields in the squirrel monkey (Saimiri sciureus). J Comp Neurol. 326:423–441.

Akbarian S, Grusser OJ, Guldin WO. 1993. Corticofugal projections to the vestibular nuclei in squirrel monkeys: further evidence

of multiple cortical vestibular fields. J Comp Neurol. 332:89–104.
Akbarian S, Grusser OJ, Guldin WO. 1994. Corticofugal connections between the cerebral cortex and brainstem vestibular nuclei in the macaque monkey. J Comp Neurol. 339:421437.
Angelaki DE. 1991. Dynamic polarization vector of spatially tuned neurons. IEEE Trans Biomed Eng. 38:1053–1060.
Angelaki DE. 1992. Spatio-temporal convergence (STC) in otolith neurons. Biol Cybern. 67:83–96.
Angelaki DE, Dickman JD. 2000. Spatiotemporal processing of linear acceleration: primary afferent and central vestibular neuron responses. J Neurophysiol. 84:2113–2132.
Angelaki DE, Shaikh AG, Green AM, Dickman JD. 2004. Neurons compute internal models of the physical laws of motion. Nature. 430:560–564.
Bremmer F, Klam F, Duhamel JR, Ben Hamed S, Graf W. 2002. Visual-vestibular interactive responses in the macaque ventral intraparietal area (VIP). Eur J Neurosci. 16:1569–1586.
Buettner UW, Buttner U, Henn V. 1978. Transfer characteristics of neurons in the vestibular nuclei of the alert monkey. J Neurophysiol. 41:1614–1628.
Büttner U, Buettner UW. 1978. Parietal cortex (2v) neuronal activity in the alert monkey during natural vestibular and optokinetic stimulation. Brain Res. 153:392–397.
Büttner U, Henn V, Oswald HP. 1977. Vestibular-related neuronal activity in the thalamus of the alert monkey during sinusoidal rotation in the dark. Exp Brain Res. 30:435–444.
Chen A, DeAngelis GC, Angelaki DE. 2010. Macaque parieto-insular vestibular cortex: responses to self-motion and optic flow. J Neurosci. 30:3022–3042.
Chen-Huang C, Peterson BW. 2006. Three dimensional spatial-temporal convergence of otolith related signals in vestibular only neurons in squirrel monkeys. Exp Brain Res. 168:410–426.
Cohen B, Matsuo V, Raphan T. 1977. Quantitative analysis of the velocity characteristics of optokinetic nystagmus and optokinetic after-nystagmus. J Physiol. 270:321–344.
Dickman JD, Angelaki DE. 2002. Vestibular convergence patterns in vestibular nuclei neurons of alert primates. J Neurophysiol. 88:3518–3533.
Dickman JD, Angelaki DE. 2004. Dynamics of vestibular neurons during rotational motion in alert rhesus monkeys. Exp Brain Res. 155:91–101.
Duffy CJ. 1998. MST neurons respond to optic flow and translational movement. J Neurophysiol. 80:1816–1827.
Fernandez C, Goldberg JM, Abend WK. 1972. Response to static tilts of peripheral neurons innervating otolith organs of the squirrel monkey. J Neurophysiol. 35:978–987.
Fredrickson JM, Scheid P, Figge U, Kornhuber HH. 1966. Vestibular nerve projection to the cerebral cortex of the rhesus monkey. Exp Brain Res. 2:318–327.
Fukushima K. 1997. Corticovestibular interactions: anatomy, electrophysiology, and functional considerations. Exp Brain Res. 117:1–16.
Fukushima K, Sato T, Fukushima J, Shinmei Y, Kaneko CR. 2000. Activity of smooth pursuit-related neurons in the monkey periarcuate cortex during pursuit and passive whole-body rotation. J Neurophysiol. 83:563–587.
Goldberg JM, Fernandez C. 1971. Physiology of peripheral neurons innervating semicircular canals of the squirrel monkey. I. Resting discharge and response to constant angular accelerations. J Neurophysiol. 34:635–660.
Green AM, Shaikh AG, Angelaki DE. 2005. Sensory vestibular contributions to constructing internal models of self-motion. J Neural Eng. 2:S164–S179.
Grüsser OJ, Pause M, Schreiter U. 1982. Neuronal responses in the parieto-insular vestibular cortex of alert Java monkeys (Macaca fascicularis). In: Roucoux A, Crommelinck M, editors. Physiological and pathological aspects of eye movements. The Hague (The Netherlands): Junk W. p. 251–270.
Grüsser OJ, Pause M, Schreiter U. 1990. Localization and responses of neurones in the parieto-insular vestibular cortex of awake monkeys (Macaca fascicularis). J Physiol. 430:537–557.
Gu Y, DeAngelis GC, Angelaki DE. 2007. A functional link between area MSTd and heading perception based on vestibular signals. Nat Neurosci. 10:1038–1047.
Gu Y, Watkins PV, Angelaki DE, DeAngelis GC. 2006. Visual and nonvisual contributions to three-dimensional heading selectivity in the medial superior temporal area. J Neurosci. 26:73–85.
Guldin WO, Akbarian S, Grusser OJ. 1992. Cortico-cortical connections and cytoarchitectonics of the primate vestibular cortex: a study in squirrel monkeys (Saimiri sciureus). J Comp Neurol. 326:375–401.
Guldin WO, Grusser OJ. 1998. Is there a vestibular cortex? Trends Neurosci. 21:254–259.
Haque A, Angelaki DE, Dickman JD. 2004. Spatial tuning and dynamics of vestibular semicircular canal afferents in rhesus monkeys. Exp Brain Res. 155:81–90.
Howard IP, Zacher JE, Allison RS. 1998. Post-rotatory nystagmus and turning sensations after active and passive turning. J Vestib Res. 8:299–312.
Kasahara M, Mano N, Oshima T, Ozawa S, Shimazu H. 1968. Contralateral short latency inhibition of central vestibular neurons in the horizontal canal system. Brain Res. 8:376–378.
Kasahara M, Uchino Y. 1974. Bilateral semicircular canal inputs to neurons in cat vestibular nuclei. Exp Brain Res. 20:285–296.
Klam F, Graf W. 2003. Vestibular response kinematics in posterior parietal cortex neurons of macaque monkeys. Eur J Neurosci. 18:995–1010.
Kornhuber HH. 1972. Vestibular influences on the vestibular and the somatosensory cortex. Prog Brain Res. 37:567–572.
Liu S, Angelaki DE. 2009. Vestibular signals in macaque extrastriate visual cortex are functionally appropriate for heading perception. J Neurosci. 29:8936–8945.
Malinvaud D, Vassias I, Reichenberger I, Rössert C, Straka H. 2010. Functional organization of vestibular commissural connections in frog. J Neurosci. 30:3310–3325.
Marlinski V, McCrea RA. 2008. Activity of ventroposterior thalamus neurons during rotation and translation in the horizontal plane in the alert squirrel monkey. J Neurophysiol. 99:2533–2545.
Meng H, Green AM, Dickman JD, Angelaki DE. 2005. Pursuit–vestibular interactions in brain stem neurons during rotation and translation. J Neurophysiol. 93:3418–3433.
Meng H, May PJ, Dickman JD, Angelaki DE. 2007. Vestibular signals in primate thalamus: properties and origins. J Neurosci. 27:13590–13602.
Mergner T, Siebold C, Schweigart G, Becker W. 1991. Human perception of horizontal trunk and head rotation in space during vestibular and neck stimulation. Exp Brain Res. 85:389–404.
Nishiike S, Guldin WO, Baurle J. 2000. Corticofugal connections between the cerebral cortex and the vestibular nuclei in the rat. J Comp Neurol. 420:363–372.
Odkvist LM, Schwarz DW, Fredrickson JM, Hassler R. 1974. Projection of the vestibular nerve to the area 3a arm field in the squirrel monkey (saimiri sciureus). Exp Brain Res. 21:97–105.
Okada T, Grunfeld E, Shallo-Hoffmann J, Bronstein AM. 1999. Vestibular perception of angular velocity in normal subjects and in patients with congenital nystagmus. Brain. 122:1293–1303.
Page WK, Duffy CJ. 2003. Heading representation in MST: sensory interactions and population encoding. J Neurophysiol. 89:1994–2013.
Ramachandran R, Lisberger SG. 2006. Transformation of vestibular signals into motor commands in the vestibuloocular reflex pathways of monkeys. J Neurophysiol. 96:1061–1074.
Raphan T, Matsuo V, Cohen B. 1979. Velocity storage in the vestibulo-ocular reflex arc (VOR). Exp Brain Res. 35:229–248.
Reisine H, Raphan T. 1992. Neural basis for eye velocity generation in the vestibular nuclei of alert monkeys during off-vertical axis rotation. Exp Brain Res. 92:209–226.
Sadeghi SG, Minor LB, Cullen KE. 2007. Response of vestibular-nerve afferents to active and passive rotations under normal conditions and after unilateral labyrinthectomy. J Neurophysiol. 97:1503–1514.
Schlack A, Hoffmann KP, Bremmer F. 2002. Interaction of linear vestibular and visual stimulation in the macaque ventral intraparietal area (VIP). Eur J Neurosci. 16:1877–1886.
Schwarz DW, Fredrickson JM. 1971. Rhesus monkey vestibular cortex: a bimodal primary projection field. Science. 172:280–281.

Shaikh AG, Ghasia FF, Dickman JD, Angelaki DE. 2005. Properties of cerebellar fastigial neurons during translation, rotation, and eye movements. J Neurophysiol. 93:853–863.
Shaikh AG, Green AM, Ghasia FF, Newlands SD, Dickman JD, Angelaki DE. 2005. Sensory convergence solves a motion ambiguity problem. Curr Biol. 15:1657–1662.
Shimazu H, Precht W. 1965. Tonic and kinetic responses of cat's vestibular neurons to horizontal angular acceleration. J Neurophysiol. 28:991–1013.
Shimazu H, Precht W. 1966. Inhibition of central vestibular neurons from the contralateral labyrinth and its mediating pathway. J Neurophysiol. 29:467–492.
Si X, Angelaki DE, Dickman JD. 1997. Response properties of pigeon otolith afferents to linear acceleration. Exp Brain Res. 117:242–250.
Takahashi K, Gu Y, May PJ, Newlands SD, DeAngelis GC, Angelaki DE. 2007. Multimodal coding of three-dimensional rotation and translation in area MSTd: comparison of visual and vestibular selectivity. J Neurosci. 27:9742–9756.
Uchino Y, Ichikawa T, Isu N, Nakashima H, Watanabe S. 1986. The commissural inhibition on secondary vestibulo-ocular neurons in the vertical semicircular canal systems in the cat. Neurosci Lett. 70:210–216.
Waespe W, Henn V. 1977. Neuronal activity in the vestibular nuclei of the alert monkey during vestibular and optokinetic stimulation. Exp Brain Res. 27:523–538.
Wilson VJ, Zarzecki P, Schor RH, Isu N, Rose PK, Sato H, Thomson DB, Umezaki T. 1999. Cortical influences on the vestibular nuclei of the cat. Exp Brain Res. 125:1–13.
Yakusheva T, Blazquez PM, Angelaki DE. 2008. Frequency-selective coding of translation and tilt in macaque cerebellar nodulus and uvula. J Neurosci. 28:9997–10009.
Yakusheva T, Blazquez PM, Angelaki DE. Forthcoming 2010. Relationship between complex and simple spike activity in macaque caudal vermis during three-dimensional vestibular stimulation. J Neurosci. 30:8111–8126.
Yakusheva TA, Shaikh AG, Green AM, Blazquez PM, Dickman JD, Angelaki DE. 2007. Purkinje cells in posterior cerebellar vermis encode motion in an inertial reference frame. Neuron. 54: 973–985.
Yakushin SB, Raphan T, Cohen B. 2006. Spatial properties of central vestibular neurons. J Neurophysiol. 95:464–478.
Zhou W, Tang BF, Newlands SD, King WM. 2006. Responses of monkey vestibular-only neurons to translation and angular rotation. J Neurophysiol. 96:2915–2930.